

Electronic Supplementary Information for

Templated synthesis of zirconium(IV)-based metal-organic layers (MOLs) with accessible chelating sites

Pol Gimeno-Fonquernie,^a Weibin Liang,^{a†} Jorge Albalad,^a Andrew Kuznicki,^c Jason R. Price,^b Eric D. Bloch,^c Christian J. Doonan^{a*} and Christopher J. Sumby^{a*}

^a Centre for Advanced Nanomaterials and Department of Chemistry, The University of Adelaide, Adelaide, SA 5000, Australia. Email: christian.doonan@adelaide.edu.au; christopher.sumby@adelaide.edu.au

^b ANSTO Melbourne, The Australian Synchrotron, 800 Blackburn Rd, Clayton, Vic 3168, Australia.

^c Department of Chemistry & Biochemistry, University of Delaware, Newark, DE 19716, USA

[†]Current address: School of Chemical and Biomolecular Engineering, Sydney Nano Institute, The University of Sydney, New South Wales, 2006, Australia.

Table of Contents

S1. Experimental	3
S1.1. Materials and Methods	3
S1.2. Synthetic protocols.....	3
S1.2.1. Synthesis of 1,1'-methylenebis(1H-pyrazole-4-carboxylic acid) (H ₂ L).....	3
S1.2.2. Synthesis of UAM-1	4
S1.2.3. Synthesis of UAM-2	4
S1.2.4. Synthesis of UAM-2·HCl.....	4
S1.2.5. Synthesis of UAM-2·ns	4
S1.2.6. General protocol for the post-synthetic metalation of UAM-1 and UAM-2	5
S2. Main text supporting characterisation.....	6
S3. Fourier Transform Infrared Spectroscopy (FTIR) spectra	16
S4. Nuclear Magnetic Resonance (NMR) data	17
S5. Single crystal X-ray crystallography	18
S5.1. General Procedures.....	18
S5.2 Specific Data and Refinement Details	18
S5.3 Thermal ellipsoid plots for all structures at the 50% probability level	20
S5.4. Crystallographic representations	21
S5.4.1. UAM-1	21
S5.4.2. UAM-2	22
S5.5 Tables of X-ray crystallography data collection and refinement parameters.....	23
S6. References.....	24

S1. Experimental

S1.1. Materials and Methods

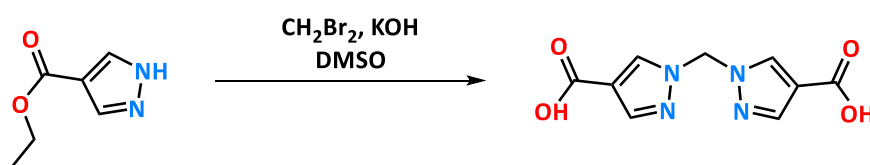
Unless otherwise stated, all chemicals were obtained from commercial sources and used as received. Acetonitrile (MeCN) was dried from CaH₂ under N₂ and degassed with Ar prior to use. The chemicals CuI, CuCl₂ anhydrous, CoCl₂ anhydrous, ZrOCl₂·8H₂O and PdCl₂ were obtained from commercial sources and used without further purification.

PXRD data were collected on a Bruker Advanced D8 diffractometer (capillary stage) using Cu K_α radiation ($\lambda = 1.5456 \text{ \AA}$, 40 kW/40 mA, $2\theta = 2\text{--}52.94^\circ$, ϕ rotation = 20 rotations/min, at 1 s exposure per step with 5001 steps, and using 0.5 mm glass capillaries). FTIR spectra were collected on a Shimadzu IR spirit spectrometer using an ATR attachment (spectral range: 7800 – 350 cm⁻¹). Nuclear Magnetic Resonance (NMR) spectra were collected at 25 °C in deuterated solvents on an Agilent DD2 500 MHz NMR with a 5 mm OneNMR probe, using tetramethylsilane (TMS) signals as the internal reference standard. Solid MOF/MOL samples were digested in NaOD/D₂O at 80 °C. SEM images were collected and EDX analysis performed on a FEI Quanta 450 field-emission scanning electron microscope, operating at 10.0 – 20.0 kV and under ultra-high vacuum (10⁻⁷ – 10⁻¹² hPa) conditions. TEM images were performed on a Tecnai G2 Spirit, operating at voltages of 20 - 120 kV and ultra-high vacuum (10⁻¹² hPa) conditions. Gas adsorption measurements were performed on a Micromeritics 3-Flex surface area and pore size analyser. Activation of samples was carried out as described in the captions of Figures S9 and S11. Geometric surface area was calculated in Materials Studio using the accessible solvent surface @1.84 Å using the relevant experimental CIF.

S1.2. Synthetic protocols

Synthesis of organic linker

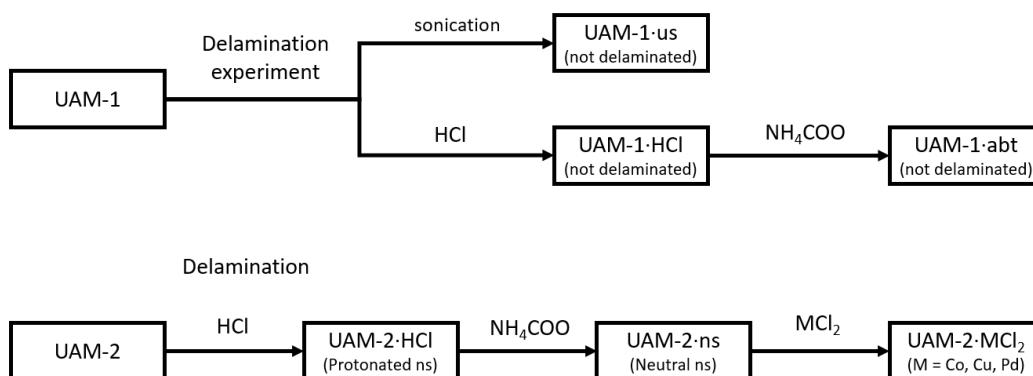
S1.2.1. Synthesis of 1,1'-methylenebis(1H-pyrazole-4-carboxylic acid) (H₂L)



Ethyl 1H-pyrazole-4-carboxylate (5.2 g, 0.037 mmol) and finely powdered potassium hydroxide (8.25 g, 0.147 mmol) were dissolved in 30 mL of DMSO, and the resulting solution was stirred for 1 h at 60 °C. After that, a solution of dibromomethane (1.3 mL, 0.019 mmol) in 10 mL of DMSO was added dropwise before being left to stir overnight at 60 °C. The solution was then poured into 200 mL of distilled water and was washed with chloroform (5 x 30 mL), and the combined organic phases were discarded. The aqueous phase was then acidified to pH = 3 with a 4 M HCl solution to precipitate H₂L as a white solid, washed with water (2 x 50 mL), and dried under vacuum for 24 h. Yield: 4.2 g (94%). FTIR ν_{max} (Nujol, cm⁻¹): 1670, 1565, 1421, 1367, 1245; ¹H NMR (500 MHz, DMSO-*d*₆): 12.49 (s, 2H, COOH), 8.50 (s, 2H, CH₂ pyrazole), 7.84 (s, 2H, CH₂ pyrazole), 6.46 (s, 2H, N-CH₂-N).

Note that a similar procedure has recently been reported by N. P. Burlutskiy *et al.*¹

Synthesis of the reported metal-organic frameworks (MOFs) and metal-organic layers (MOLs)



Scheme S1. A schematic showing the naming of all the metal-organic compounds mentioned in the manuscript.

S1.2.2. Synthesis of UAM-1

A solution of $\text{ZrOCl}_2 \cdot 8\text{H}_2\text{O}$ (32 mg, 0.10 mmol) and formic acid (0.6 mL, 15.90 mmol, 171 mol. eq.) in 1 mL of DMF was sonicated for 30 min. Separately, H_2L (25 mg, 0.11 mmol) was dissolved in 0.9 mL of DMF and sonicated until solution. Then, the ligand solution was added to the metal precursor one, and the resulting mixture was transferred to a solvothermal scintillation vial and heated at 120 °C for 48 h. Single-crystals of **UAM-1** were separated by filtration and washed with DMF (4 x 5 mL), acetone (3 x 5 mL), and dried under vacuum for 24 h.

S1.2.3. Synthesis of UAM-2

$\text{ZrOCl}_2 \cdot 8\text{H}_2\text{O}$ (25 mg, 0.08 mmol), H_2L (25 mg, 0.11 mmol) and CuI (25 mg, 0.13 mmol) were dissolved in 1.5 mL of DMF and sonicated for 30 min. Formic acid (0.8 mL, 21.10 mmol, 273 mol. eq.) was then added to the solution, and the resulting mixture was transferred to a solvothermal scintillation vial and heated at 120 °C for 48 h. Microcrystalline **UAM-2** was collected by filtration and washed with DMF (4 x 5 mL), acetone (3 x 5 mL) and dried under vacuum for 24 h.

To obtain single crystals suitable for X-ray crystallography, the procedure was slightly modified as follows. The same quantities of reagents and solvent were thoroughly mixed, transferred to a non-solvothermal vial (with pressure regulation), and heated at 140 °C for 48 h. Single crystals of **UAM-2** were collected by filtration, and washed with DMF (3 x 5 mL).

S1.2.4. Synthesis of UAM-2·HCl

UAM-2 (50 mg, 0.025 mmol) was soaked in a 5 mL stock solution of HCl in DMF (1.3 mL 4 M HCl in 29.7 mL DMF) and heated to 60 °C for 48 h to induce the acid-triggered chemical delamination of the sample. **UAM-2·HCl** was then collected by centrifugation and thoroughly washed with DMF (4 x 5 mL). For characterisation, the sample was washed with acetone (3 x 5 mL) and dried under reduced pressure overnight.

S1.2.5. Synthesis of UAM-2·ns

UAM-2·HCl (50 mg, 0.026 mmol) was neutralised with a 0.05 M ammonium formate solution in MeOH (5 x 5 mL). The solution was left to stand at room temperature for 16 h and the supernatant was exchanged with fresh DMF twice over 24 h.

S1.2.6. General protocol for the post-synthetic metalation of UAM-1 and UAM-2

The different phases of **UAM-1** or **UAM-2·ns** (50 mg, 0.028 mmol) were soaked in 3 mL of dry acetonitrile. An excess of metal salt (~20 mg of PdCl₂, CuCl₂, or CoCl₂) was added, and the solution was heated to 60 °C for 2 h, 5 h or 24 h. The sample was then washed by decantation with dry acetonitrile (4 x 4 mL).

S2. Main text supporting characterisation

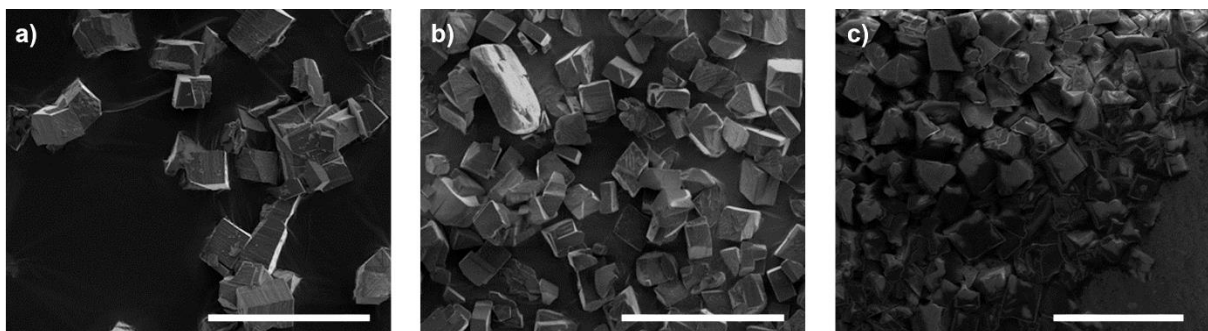


Figure S1. a) SEM images of (a) **UAM-1** as made, (b) **UAM-1** after 2 h under sonication, and (c) **UAM-1·HCl**. (Scale bar= 50 μm).

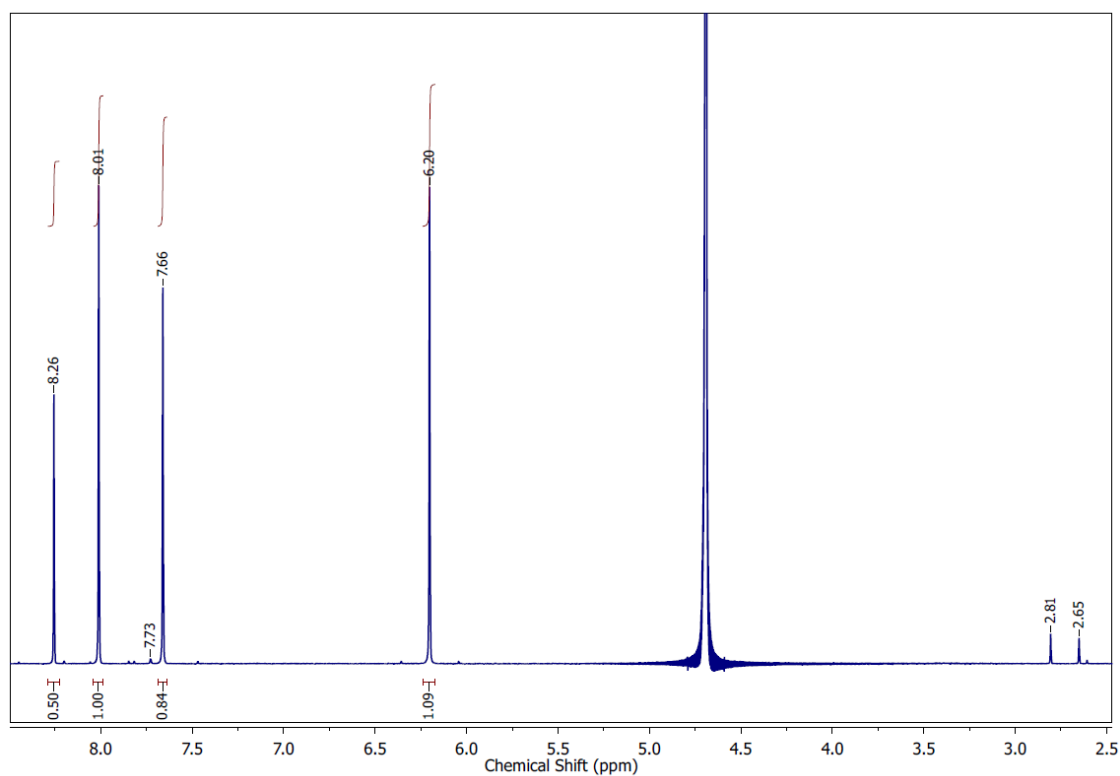


Figure S2. ^1H -NMR spectrum of digested **UAM-1**. Digestion conditions: 50 μL NaOD in 500 μL of D_2O , heated at 80 $^\circ\text{C}$ for 1 h. Sample preparation: **UAM-1** was washed with DMF (4 x 5 mL), acetone (3 x 5 mL) and dried under vacuum for 24 h. Digestion conditions: 50 μL NaOD in 500 μL of D_2O , heated at 80 $^\circ\text{C}$ for 1 h. Peak at 8.26 ppm corresponds to the formate anion. Its relative integration compared with the L peaks show a molar ratio L:formate 1:1 which is consistent with four L and four formate anions linked to each Zr cluster. Peaks at 7.73, 2.81 and 2.65 show the presence of some DMF trapped in the structure.

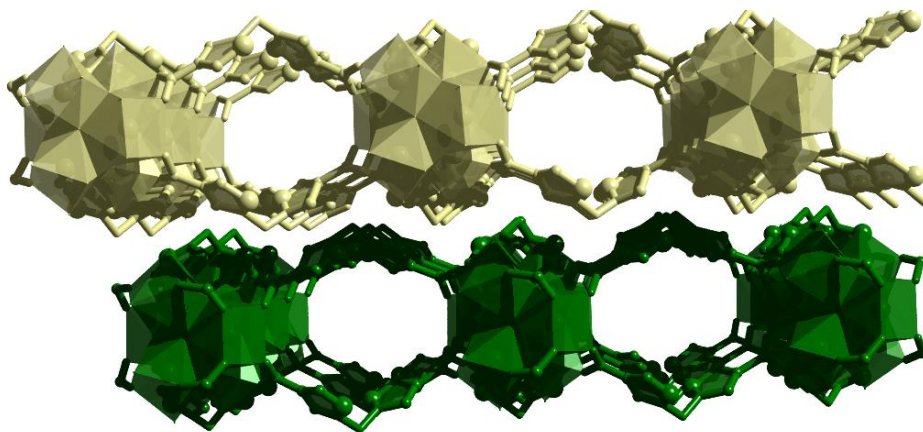


Figure S3. Representation of the interlayer packing in **UAM-1**.

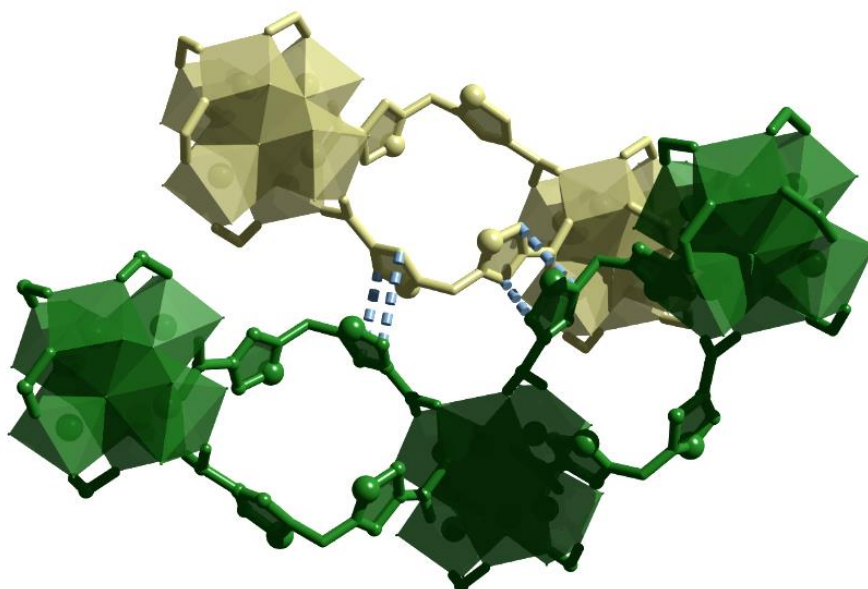


Figure S4. A close-up of the π - π interactions between vicinal pyrazoles of two **UAM-1** layers.

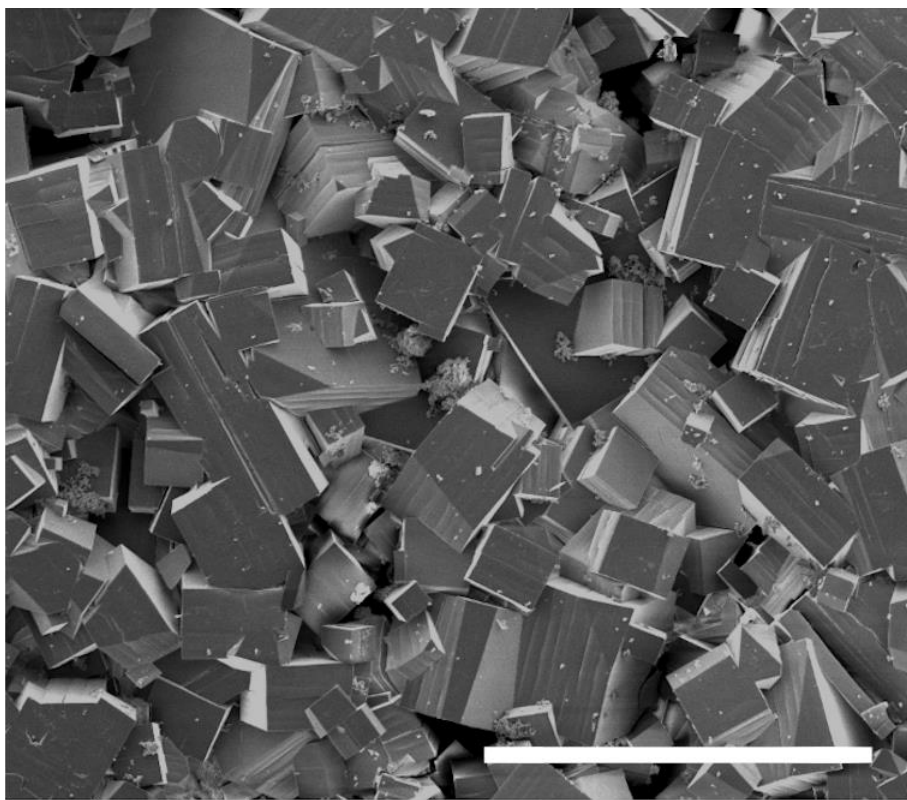


Figure S5. SEM image of **UAM-2** as made (scale bar= 50 μm).

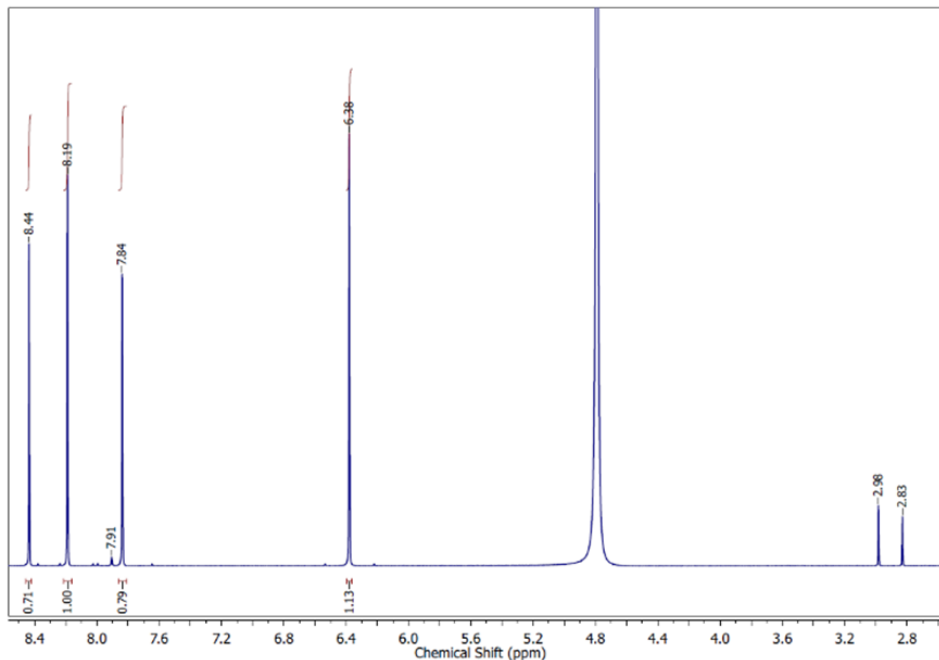


Figure S6. ^1H -NMR spectrum of digested **UAM-2**. Sample preparation: **UAM-2** was washed with DMF (4 x 5 mL), acetone (3 x 5 mL) and dried under vacuum for 24 h. Digestion conditions: 50 μL NaOD in 500 μL of D_2O , heated at 80 $^\circ\text{C}$ for 1 h. The peak at 8.31 ppm corresponds to the formate anion. Its relative integration compared with the L peaks show a molar ratio L:formate 1:1.4 which is consistent with the presence of 5.5 formate anions per Zr cluster suggesting that some of the formate anions are monodentate. Peaks at 7.91, 2.98 and 2.83 ppm show the presence of DMF molecules trapped in the structure.

Table S1. Energy-dispersive X-ray (EDX) data for Cu, I, and Cl after acid and base exfoliation treatments of **UAM-2**. Quantification of % occupancy on the bis(pyrazolyl)methane coordinating sites was determined by measuring Zr:Cu, Cu:I and Zr:Cl ratios.

Sample	Cu (% occupancy) ^{a,b}	I (% occupancy) ^{a,b}	Cl (% occupancy) ^{a,b}
UAM-2	100 ± 5	98 ± 4	6 ± 1
UAM-2·HCl	No detectable Cu	No detectable I	108 ± 5
UAM-2·ns	No detectable Cu	No detectable I	No detectable Cl

^aAverage atomic% obtained from three areas of three different crystals.

^bRelative to full occupancy of the bis(pyrazolyl)methane sites in **UAM-2** (Zr:Cu:I = 3:2:2) and **UAM-2·ns** (Zr:Cl = 3:2).

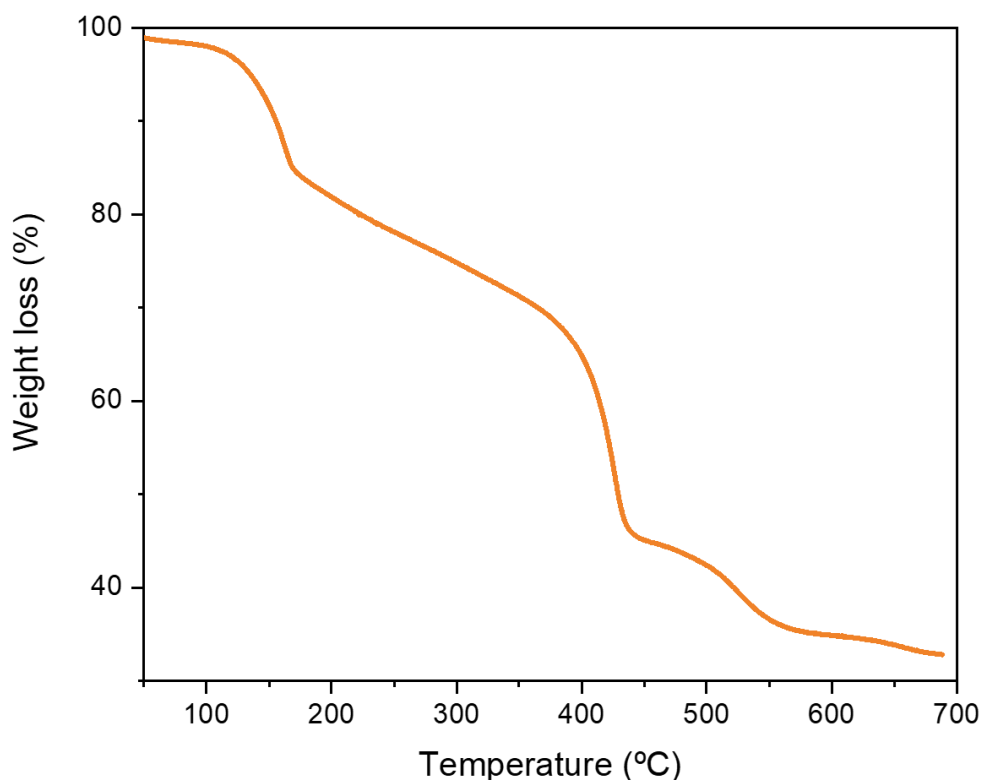


Figure S7. Thermogravimetric analysis spectrum (orange) of **UAM-1**. Analysis conditions: 50 °C – 700 °C at 5 °C/min, under an oxidising (air) atmosphere.

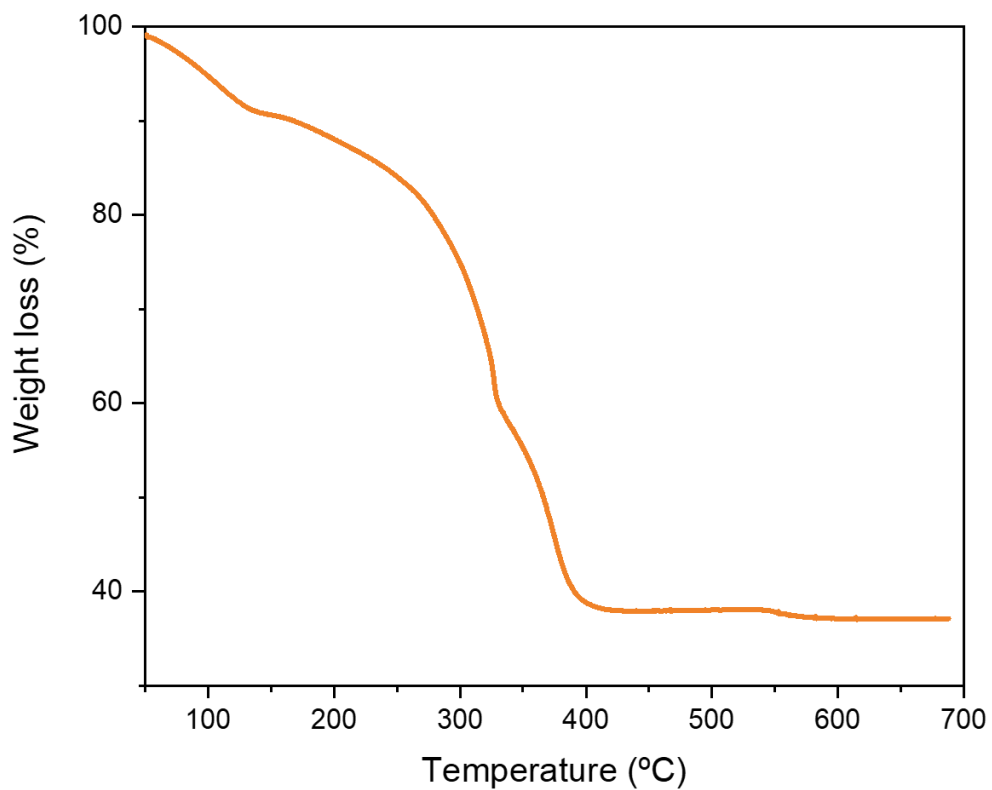


Figure S8. Thermogravimetric analysis spectrum (orange) of **UAM-2**. Analysis conditions: 50 °C – 700 °C at 5 °C/min, under an oxidising (air) atmosphere.

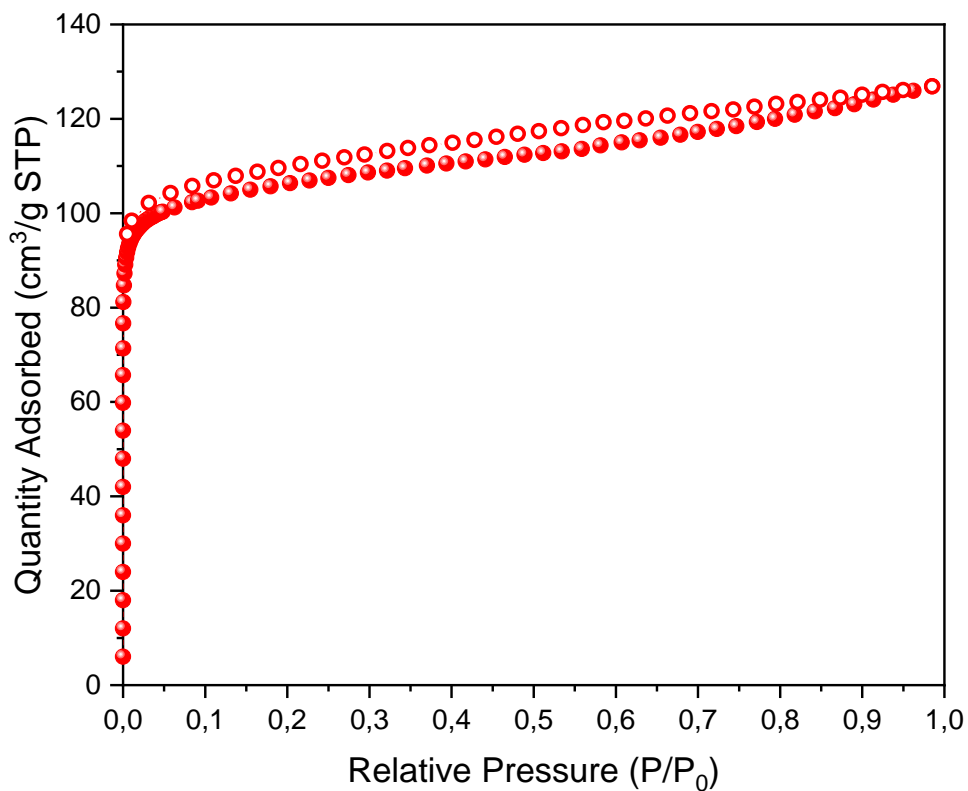


Figure S9. 77 K N₂ isotherm data of **UAM-1**, after activation from methanol at 120 °C for 3 h. Coloured circles represent adsorption, open circles represent desorption.

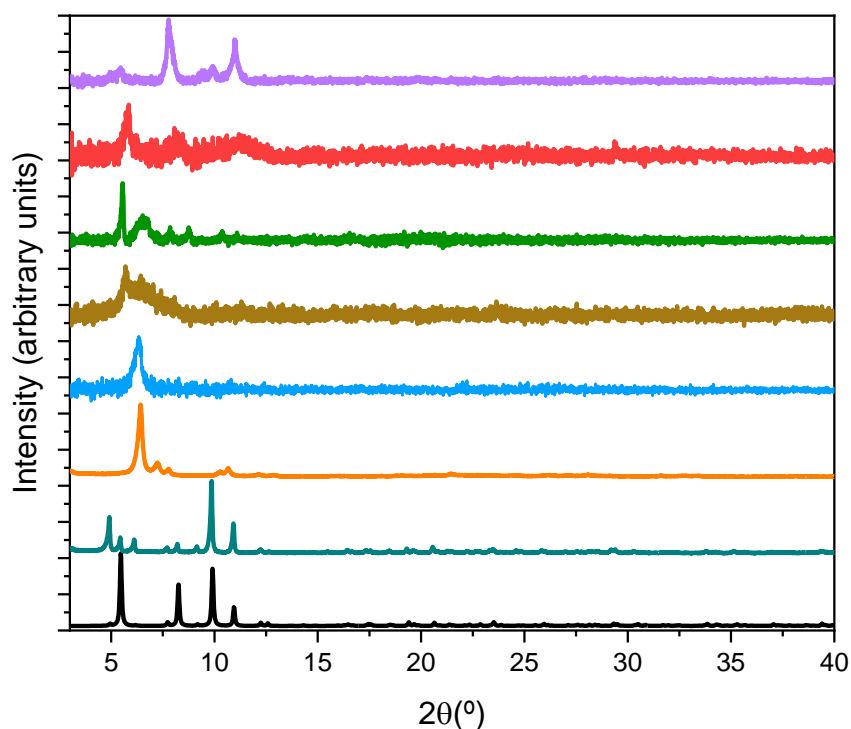


Figure S10. Experimental PXRD plots for **UAM-2** as made (green), **UAM-2·HCl** (orange), **UAM-2·ns** (blue), **UAM-2·CoCl₂** (gold), **UAM-2·CuCl₂** (green), **UAM-2·PdCl₂** (gold), and **UAM-2** after BET analysis (purple) versus simulated **UAM-2** (black).

Like other related materials with flexible linkers, the flexibility of this structure, coming from both the linker and the chemically sensitive Cu_2I_2 bridges, appears to cause slight peak shifts and changes of intensity in the PXRD peak positions. For the experimental structure versus the simulated pattern, these changes are pronounced for the crystallographic planes (110), (220) and (112), that are perpendicular or diagonal to the planes of the Cu_2I_2 bridges that connect the layers of the material and are associated with the inherent flexibility of the Cu_2I_2 bridges.

Additionally, upon changes in the solvent and loss of solvent during sample preparation for PXRD, further dramatic changes in peak position and intensity are observed. For the delaminated materials (**UAM-2·HCl** (orange) and **UAM-2·ns** (blue)), their post-synthetically metalated products and the activated material (also partially delaminated), the PXRD patterns change dramatically due to significant loss of long-range order in most crystallographic directions.

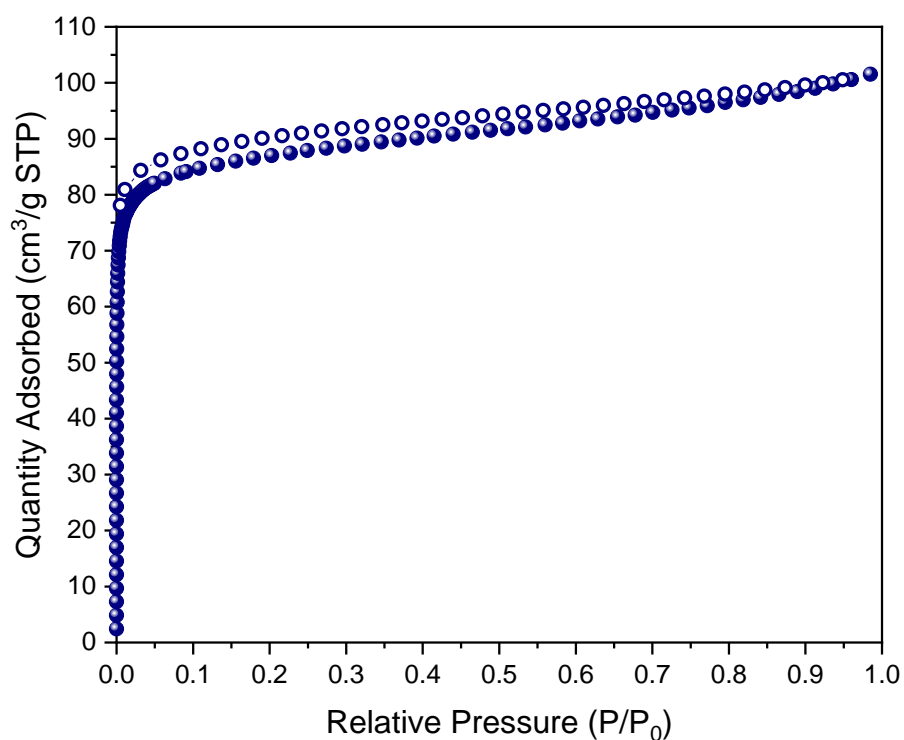


Figure S11. 77 K N₂ isotherm data of **UAM-2**, after activation from methanol at 120 °C for 3 h. Coloured circles represent adsorption, open circles represent desorption.

Table S2. Energy-dispersive X-ray (EDX) data for Co and Cl after metalation of **UAM-1** at different times. Quantification of % occupancy on the bis(pyrazolyl)methane coordinating sites was determined by measuring Zr:Co and Zr:Cl ratios.

Sample	Co (% occupancy) ^{a,b}	Cl (% occupancy) ^{a,b}
UAM-1	No detectable Co	No detectable Cl
UAM-1·CoCl₂ 2 h	4 ± 3	8 ± 4
UAM-1·CoCl₂ 5 h	3 ± 3	7 ± 5
UAM-1·CoCl₂ 24 h	4 ± 3	8 ± 4

^aAverage atomic% obtained from three areas of five different crystals.

^bRelative to full occupancy of the bis(pyrazole)methane coordinating sites in **UAM-1** (Zr:Co = 3:2).

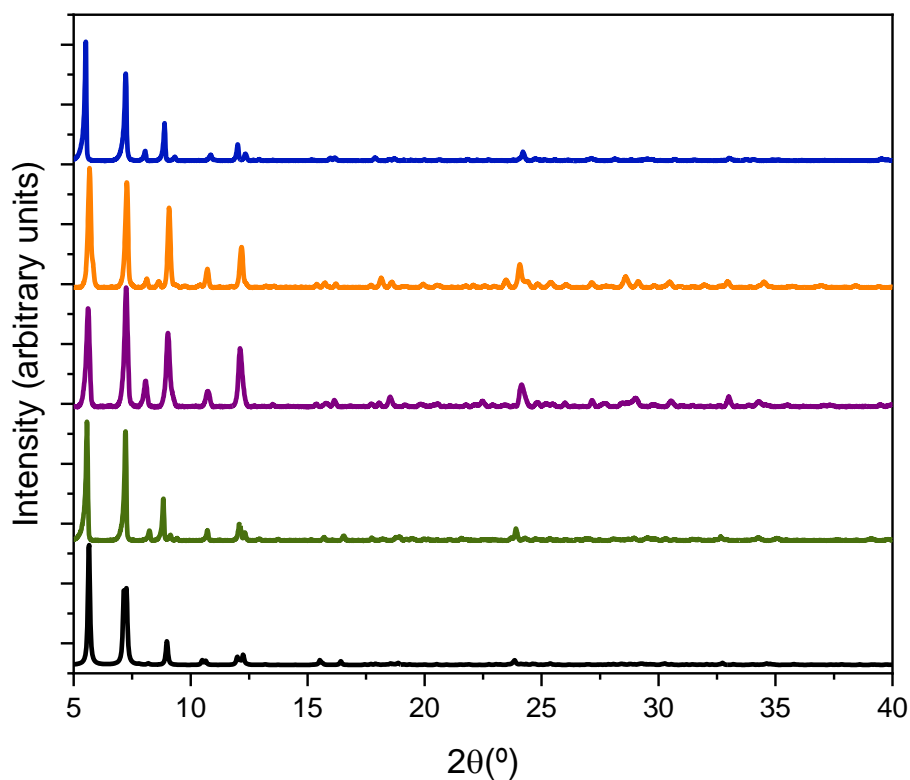


Figure S12. Experimental PXRD plots for **UAM-1 as made** (green), **UAM-1 sonicated** (purple), **UAM-1 after acid-base treatment** (orange) and **UAM-1·CoCl₂** (blue), versus simulated **UAM-1** (black). Like other related materials with flexible linkers, the flexibility of the framework appears to cause slight shifts in the PXRD peak positions upon changes in the solvent and loss of solvent during sample preparation for PXRD.

Table S3. Energy-dispersive X-ray (EDX) data for Co and Cl after metalation of “delaminated” UAM-1 at different times. Quantification of % occupancy on the bis(pyrazolyl)methane coordinating sites was determined by measuring Zr:Co and Zr:Cl ratios.

Sample	Co, (% occupancy) ^{a,b}	Cl, (% occupancy) ^{a,b}
UAM-1	No detectable Co	No detectable Cl
UAM-1·HCl	No detectable Co	104 ± 3
UAM-1·abt	No detectable Co	No detectable Cl
UAM-1·abt·CoCl₂ 2 h	3 ± 3	7 ± 3
UAM-1·abt·CoCl₂ 5 h	3 ± 4	6 ± 5
UAM-1·abt·CoCl₂ 24 h	3 ± 3	6 ± 4

^aAverage atomic% obtained from three areas of three different crystals.

^bRelative to full occupancy of the bis(pyrazole)methane coordinating sites in **UAM-1** (Zr:Co = 3:2).

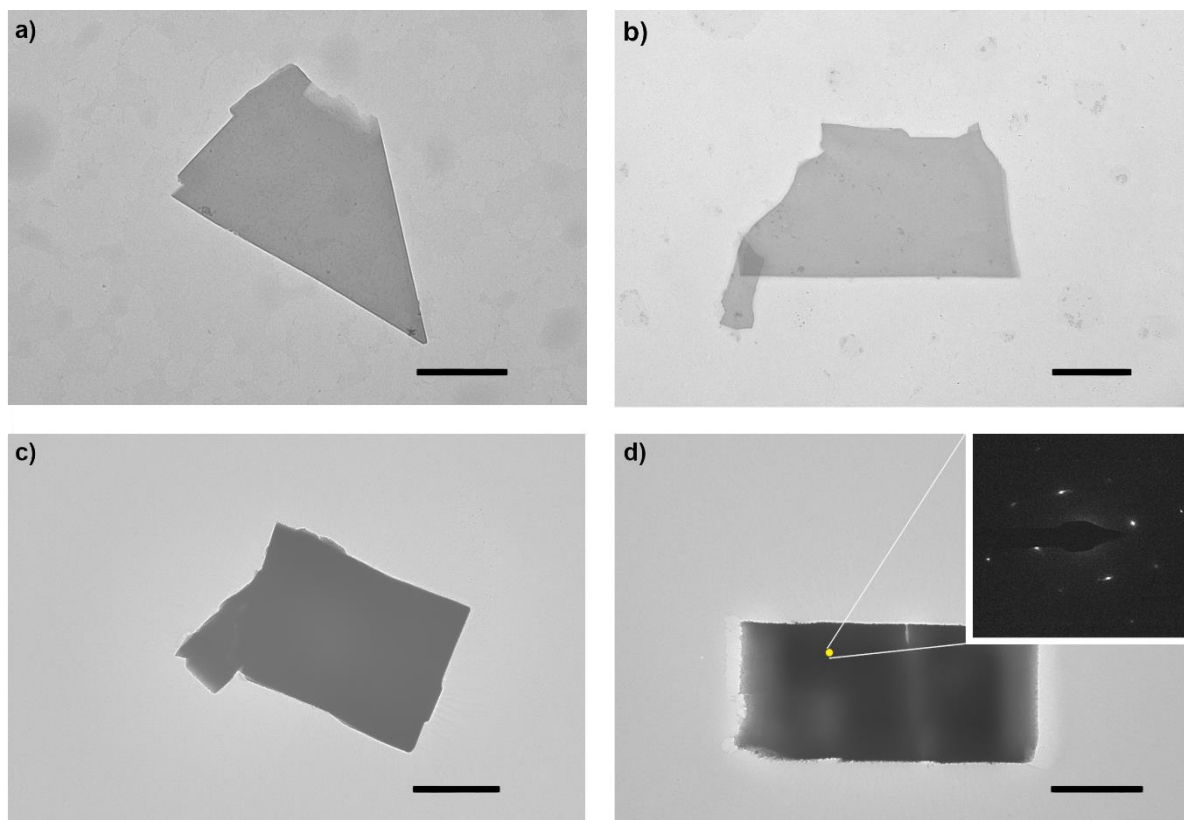


Figure S13. TEM images of **UAM-2·HCl** (a, b), TEM image of **UAM-2·ns** (c) and TEM image of **UAM-2·ns** with an inset showing a selected area electron diffraction (SAED) image demonstrating that long range order is present in the nanosheets (d). Scale bar= 1 μm .

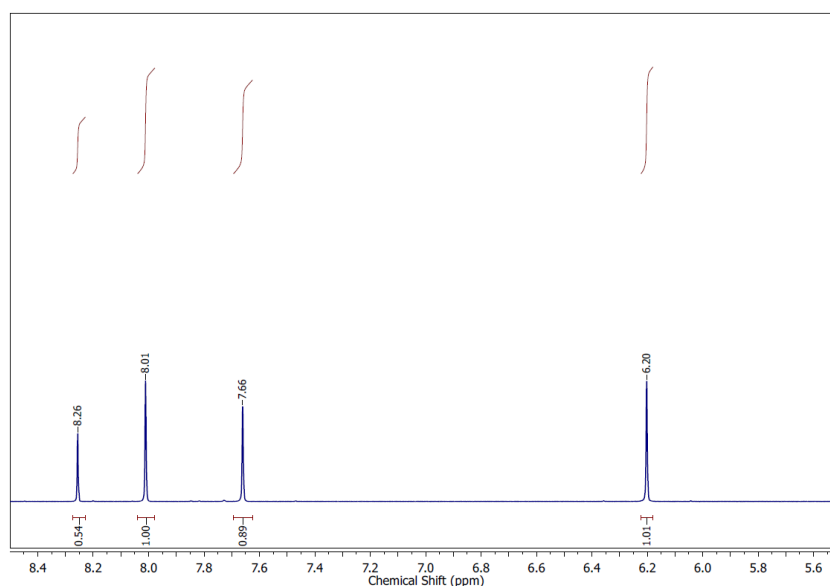


Figure S14. ¹H-NMR spectrum of **UAM-2·HCl** after NaOD/D₂O digestion. Digestion conditions: 50 μL NaOD in 500 μL of D₂O heated at 80 $^{\circ}\text{C}$ for 1 h. Peak at 8.26 ppm corresponds to the formate anion. Its relative integration compared with the L peaks show a decrease of formate anions compared to **UAM-2** with molar ratio L:formate 1:1 which is consistent with the presence of four formate anions per Zr cluster suggesting that all formates are now bidentate.

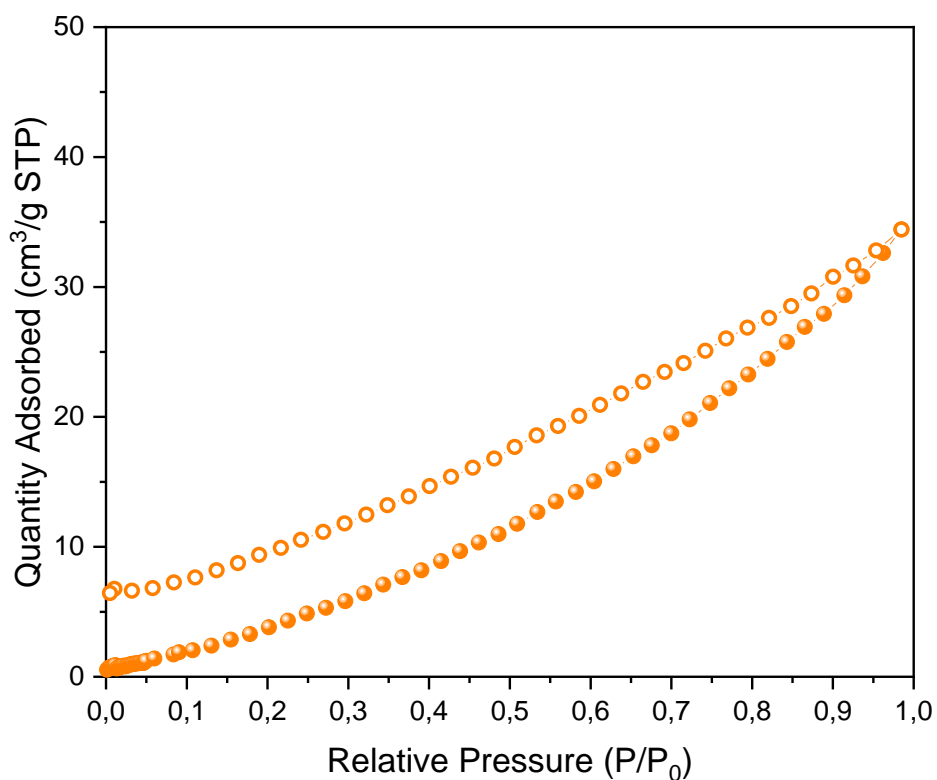


Figure S15. 77 K N₂ isotherm data of **UAM-2·ns**, after activation from methanol at 120 °C for 3 h (identical conditions to the non-delaminated material). Coloured circles represent adsorption, open circles represent desorption.

Table S4. Energy-dispersive X-ray (EDX) data for the metalation of **UAM-2** at different interval times. Quantification of % occupancy on the bis(pyrazolyl)methane coordinating sites was determined by measuring Zr:Co, Zr:Cu, Zr:Pd and Zr:Cl ratios.

Sample	Co (% occupancy) ^{a,b}	Cu (% occupancy) ^{a,b}	Pd (% occupancy) ^{a,b}	Cl (% occupancy) ^{a,b}
UAM-2·CoCl₂ 2 h	99 ± 6	No detectable	No detectable	212 ± 1
UAM-2·CoCl₂ 5 h	99 ± 5	No detectable	No detectable	213 ± 2
UAM-2·CoCl₂ 24 h	97 ± 3	No detectable	No detectable	205 ± 2
UAM-2·CuCl₂ 2 h	No detectable	98 ± 4	No detectable	200 ± 2
UAM-2·CuCl₂ 5 h	No detectable	99 ± 4	No detectable	205 ± 4
UAM-2·CuCl₂ 24 h	No detectable	103 ± 5	No detectable	201 ± 4
UAM-2·PdCl₂ 2 h	No detectable	No detectable	93 ± 3	186 ± 3
UAM-2·PdCl₂ 5 h	No detectable	No detectable	99 ± 5	201 ± 3
UAM-2·PdCl₂ 24 h	No detectable	No detectable	101 ± 4	201 ± 4

^aAverage atomic% obtained from three areas of three different crystals.

^bRelative to full occupancy of the bis(pyrazole)methane coordinating sites in **UAM-2·ns** (Zr:Co:Cl = 3:2:4; Zr:Cu:Cl = 3:2:4; Zr:Pd:Cl = 3:2:4).

S3. Fourier Transform Infrared Spectroscopy (FTIR) spectra

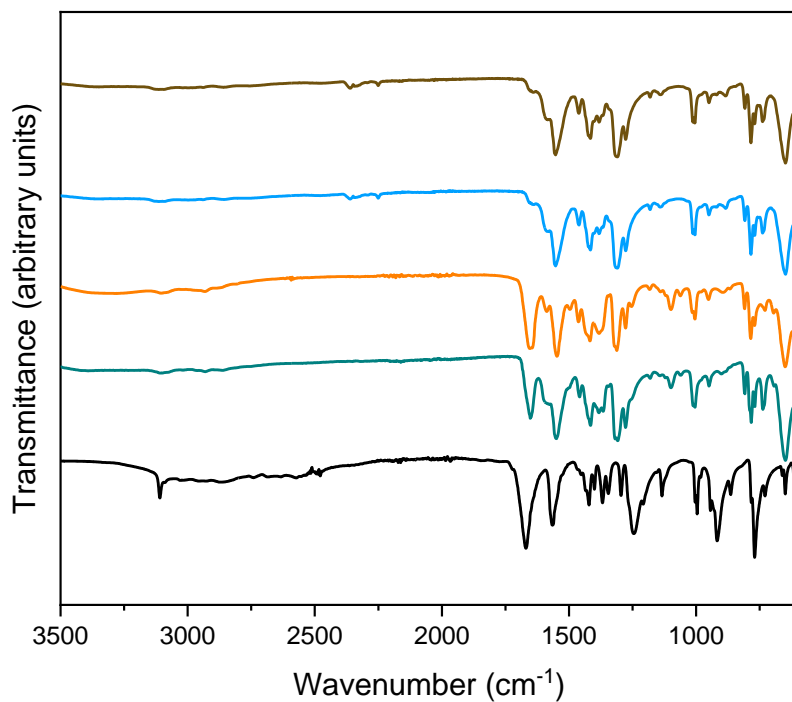


Figure S15. FTIR spectra of **H₂L** (black), **UAM-1** as made (green), **UAM-1·HCl** (orange), **UAM-1** after base (blue) and **UAM-1·CoCl₂** after sonication (brown).

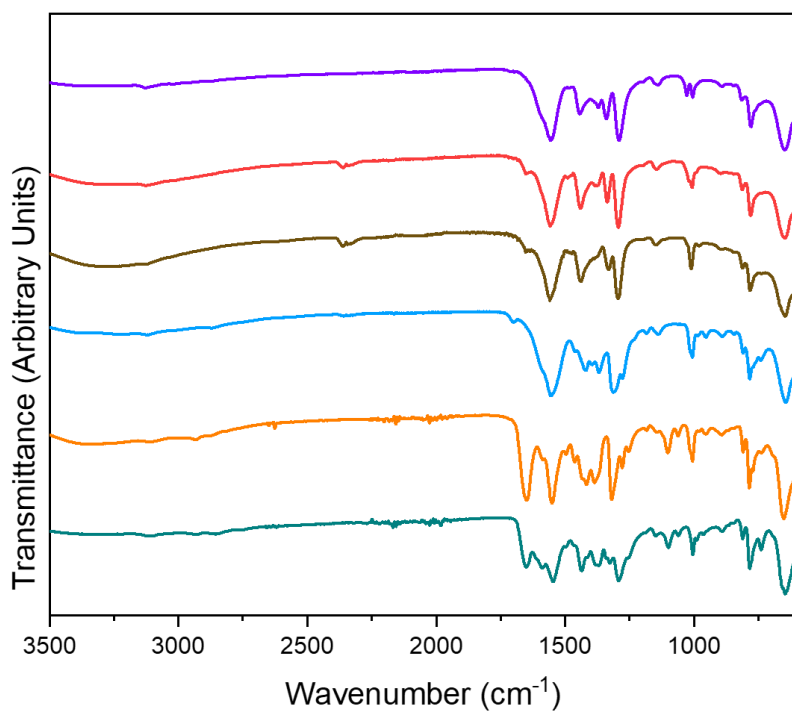


Figure S16. FTIR spectra of **UAM-2·CuI** (green), **UAM-2·HCl** (orange), **UAM-2** (blue), **UAM-2·CoCl₂** (brown), **UAM-2·CuCl₂** (red) and **UAM-2·PdCl₂** (purple).

S4. Nuclear Magnetic Resonance (NMR) data

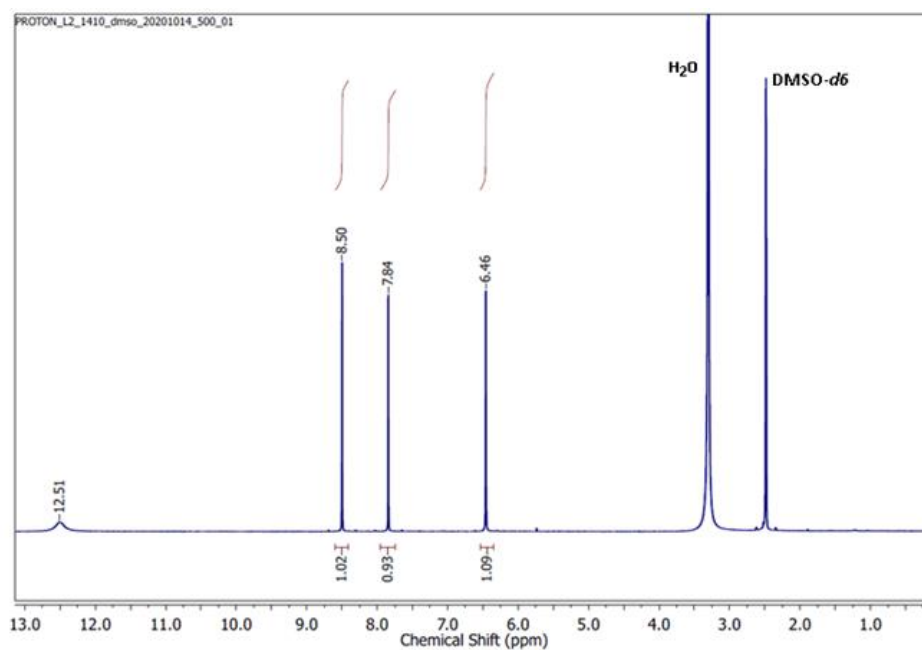


Figure S17. ¹H-NMR spectrum of H₂L.

S5. Single crystal X-ray crystallography

S5.1. General Procedures

Single crystals were mounted in Paratone-N oil on a MiTeGen micromount. Single-crystal X-ray data were typically collected at 100 K on the MX1 or MX2 beamlines of the Australian Synchrotron using the Blue-ice software interface,² $\lambda = 0.71073 \text{ \AA}$ (0.6888 \AA in the case of the provided structure of **UAM-1**). Absorption corrections were applied using multiscan methods using XDS,^{3,4} the structures solved using SHELXS or SHELXT,^{5,6} and refined by full-matrix least squares on F^2 by SHELXL,⁷ interfaced through the program X-Seed or OLEX.^{8,9} In general, all atoms were refined anisotropically and hydrogens atoms were included as invariants at geometrically estimated positions, unless specified otherwise in additional details in supporting information. Where noted, the data was treated with the SQUEEZE routine available in Platon⁹ or using the solvent masking feature of Olex. Figures were produced using the program Diamond. X-ray experimental data is given in Table S5. CIF data have been deposited with the Cambridge Crystallographic Data Centre, CCDC reference numbers CCDC 2119441 and 2119442.

S5.2 Specific Data and Refinement Details

UAM-1. There was significant ambiguity in the correct unit cell and symmetry (Bravais lattice and space group) needed to solve the structure of **UAM-1**. Many data collections and structure solutions were tried but significant residual electron density remained around the Zr atoms of the Zr-oxo cluster. This residual electron density was consistent with the structure being disordered but, despite recognising this, it remained difficult to get a chemical sensible model of the structure in the space groups identified. To identify the correct symmetry, we collected data at energies around the Zr adsorption edge (which is close to the standard Mo $K\alpha$ wavelength). Using this data, which was collected in low angle and high angle runs before being merged (using corrected scattering factors), we were able to identify an orthorhombic *Amm2* space group. Structure solution and close examination of the layer structure of the well resolved layer allowed us to identify to distinct positions of the second layer, which were refined with a 50:50 disorder model using a TWIN refinement (TWIN law -1 0 0 0 -1 0 0 0 -1).

Refinement of a sensible structural model required the use of SIMU/RIGU commands for the Zr-oxo cluster of the disordered layer, and the associated linker pyrazole rings. The pyrazole rings of L are all anti in the structure, and this gives 4-connected layers with a spacing of the Zr-oxo clusters consistent with the primary layer. A significant number of DFIX restraints were used to maintain chemically sensible bond lengths and angles for the pyrazole carboxylates and a disordered formate anion (50:50 disorder). A DMF solvate molecule was refined with isotropic displacement parameters. A solvent mask was calculated and 498 electrons were found in a volume of 3022 \AA^3 in 1 void per unit cell. This is consistent with the presence of 1.5[C₃H₇NO] (DMF) per Asymmetric Unit which account for 480 electrons per unit cell.

UAM-2. Due to the high symmetry structure the exact formulation of the Zr-oxo cluster cannot be determined (OH and O groups occupy the same positions) and the formate modulators, that were identified by digestion of the sample and NMR spectroscopy, cannot be located. Additionally, a highly disordered Zr formate cluster was identified in the structure of crystals of **UAM-2** made via the second procedure (bulk crystals made by the primary procedure do not have the second cluster that stabilises the growth of larger single crystals). A solvent mask was calculated and 4310 electrons were found in a volume of 807 \AA^3 in 1 void per unit cell. This is

consistent with the presence of $1[\text{Zr}_6\text{C}_{12}\text{H}_{16}\text{O}_{32}]$ (a disordered Zr formate cluster) per Unit Cell which account for 4672 electrons per unit cell.

S5.3 Thermal ellipsoid plots for all structures at the 50% probability level

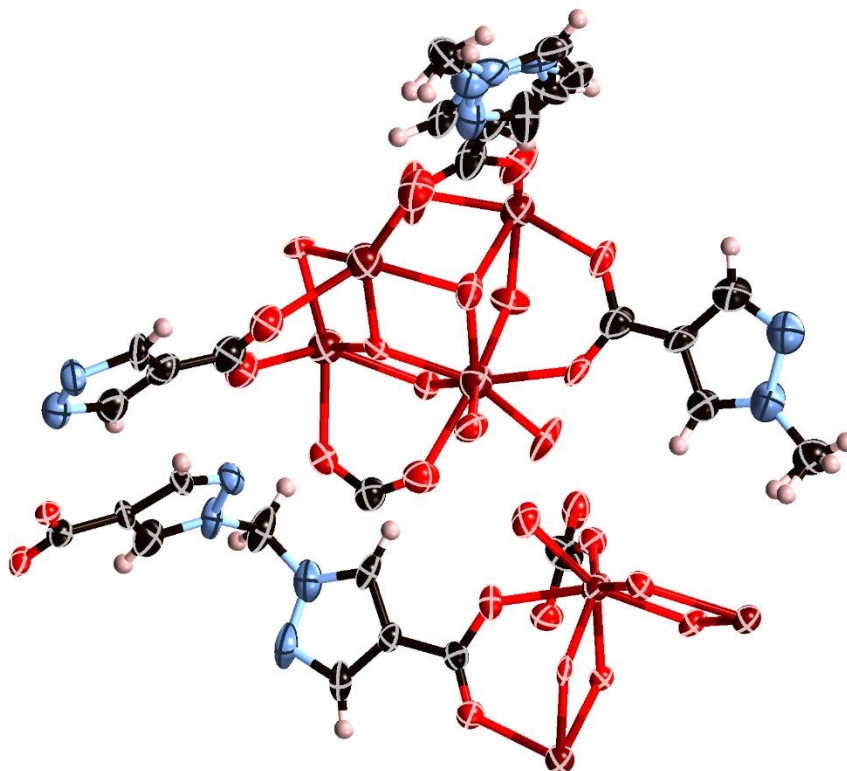


Figure S18. Asymmetric unit of **UAM-1**, with all non-hydrogen atoms represented by ellipsoids at the 50% probability level (C, black; H, pink; N, light blue; O, red; Cu, dark blue; Zr, dark red; I, purple).

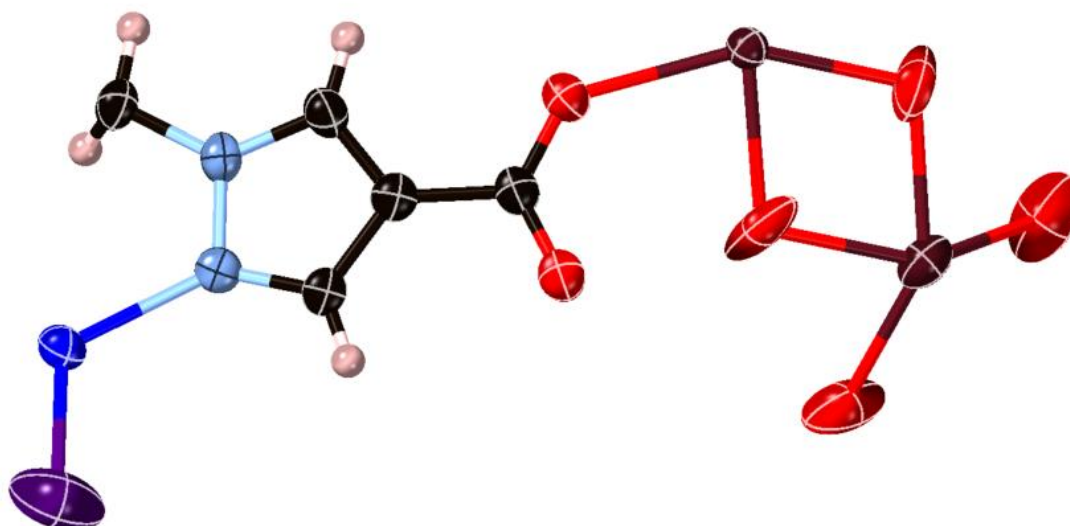


Figure S19. Asymmetric unit of **UAM-2**, with all non-hydrogen atoms represented by ellipsoids at the 50% probability level (C, black; H, pink; N, light blue; O, red; Cu, dark blue; Zr, dark red; I, purple).

S5.4. Crystallographic representations

S5.4.1. UAM-1

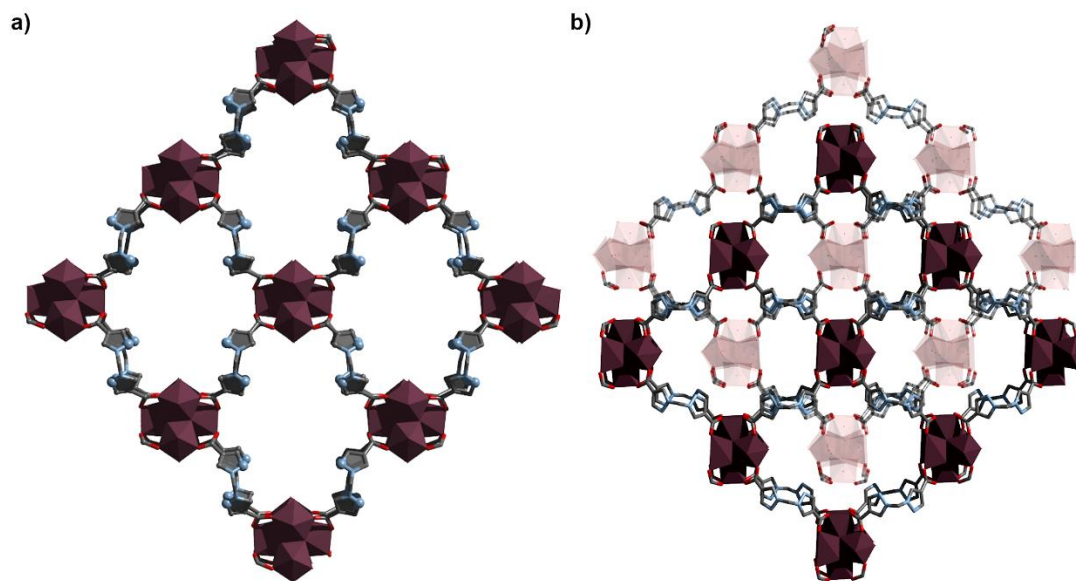


Figure S20. a) Top view crystallographic representation of a single layer of **UAM-1**. b) Top view crystallographic representation of the two different positions of the disordered layer of **UAM-1**. (C, grey; N, light blue; O, red; Zr, dark red). Hydrogens have been hidden for clarity.

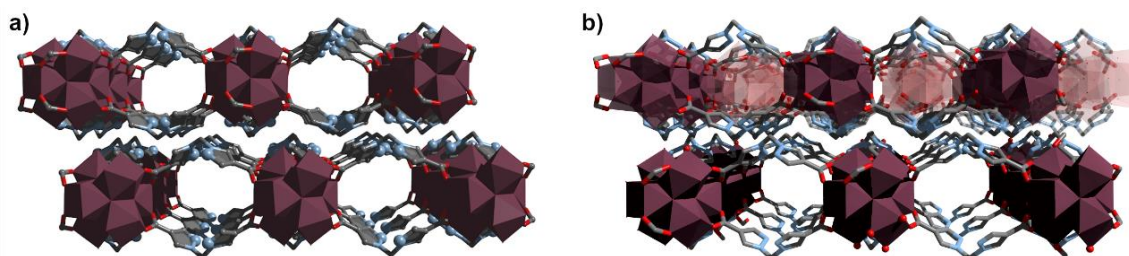


Figure S21. a) Side view crystallographic representation of two layers of **UAM-1**. b) Side view crystallographic representation of two layers of **UAM-1**. The top layer can occupy two different positions. One of the layer positions is shaded for clarity. (C, grey; N, light blue; O, red; Zr, dark red). Hydrogens have been hidden for clarity.

S5.4.2. UAM-2

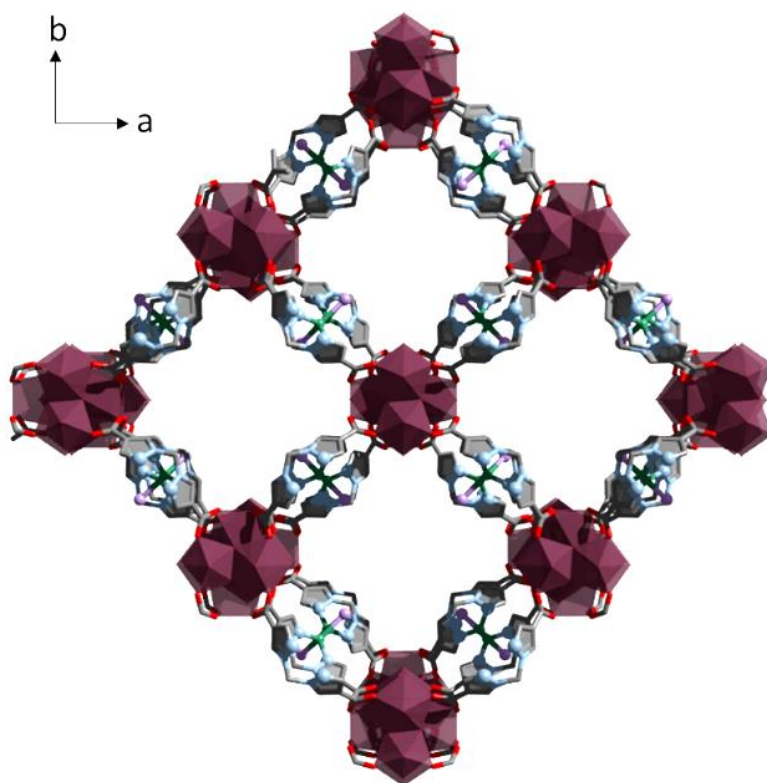


Figure S22. *ab* plane crystallographic representation of **UAM-2** (C, grey; N, light blue; O, red; Cu, green; Zr, dark red; I, pink). Hydrogens have been hidden for clarity.

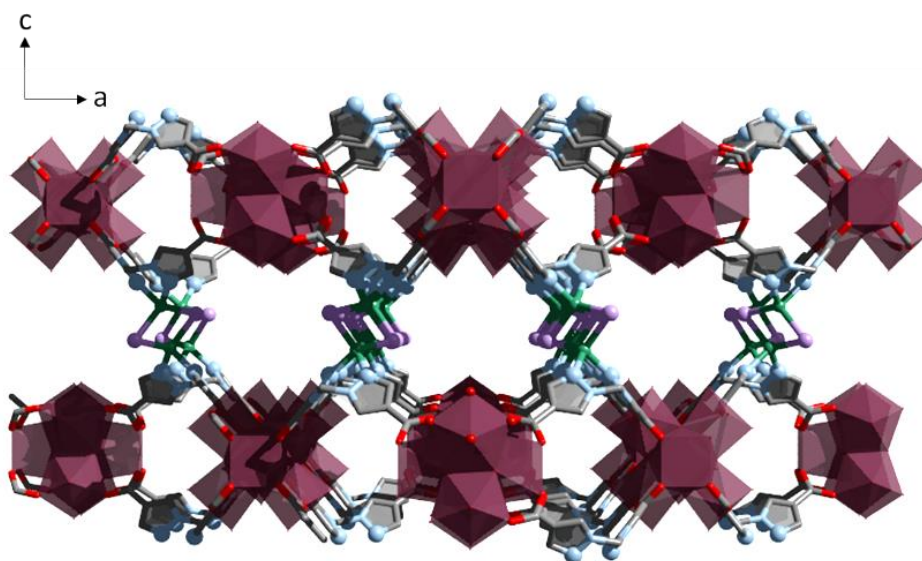


Figure S23. *ac* plane crystallographic representation of **UAM-2** (C, grey; N, light blue; O, red; Cu, green; Zr, dark red; I, pink). Hydrogens have been hidden for clarity.

S5.5 Tables of X-ray crystallography data collection and refinement parameters

Table S5. Crystallographic data collection and refinement parameters for **UAM-1** and **UAM-2**.

Sample	UAM-1	UAM-2
Crystallographic Parameter		
Formula	C _{20.5} H _{15.5} N _{8.5} O _{16.5} Zr ₃	C ₁₈ H ₁₂ Cu ₂ l ₂ N ₈ O ₁₆ Zr ₃
FW	1027.59	1250.90
T, K	100(2)	100
Wavelength, Å	Synchrotron ($\lambda = 0.6888$)	Synchrotron ($\lambda = 0.71073$)
Crystal system, space group	Orthorhombic, <i>Amm</i> 2	Tetragonal, <i>I4/mmm</i>
Z	8	8
a, Å	19.017(4)	22.738(3)
b, Å	23.361(5)	22.738(3)
c, Å	21.208(4)	28.593(6)
α , °	90	90
β , °	90	90
γ , °	90	90
V, Å ³	9422(3)	14783(5)
d_{calc} , g/cm ³	1.449	1.124
Absorption coefficient, mm ⁻¹	3.828	1.846
F(000)	4040.0	4704.0
Crystal size, mm ³	0.02 × 0.02 × 0.02	0.03 × 0.03 × 0.03
2 θ range for data collection	2.076 to 58.346	2.288 to 58.152
Index range	-23 ≤ h ≤ 23, -28 ≤ k ≤ 30, -28 ≤ l ≤ 29	-30 ≤ h ≤ 30, -31 ≤ k ≤ 30, -38 ≤ l ≤ 39
Reflections collected	106441	95189
Independent reflections	12746 [R _{int} = 0.0619, R _{sigma} = 0.0418]	4771 [R _{int} = 0.0280, R _{sigma} = 0.0080]
Data/restraints/parameters	12746/442/601	4771/0/125
GOF on F ²	1.183	1.079
Largest diff. peak and hole, eÅ ⁻³	1.34/-1.30	1.35/-2.37
R ₁ , [I > 2 σ (I)]	0.0855	0.0740
wR ₂ , all data	0.2837	0.2306
CCDC Number	2119441	2119442

S6. References

1. N. P. Burlutskiy and A. S. Potapov, *Molecules*, 2021, **26**, 413.
2. T. McPhillips, S. McPhillips, H. Chiu, A. E. Cohen, A. M. Deacon, P. J. Ellis, E. Garman, A. Gonzalez, N. K. Sauter, R. P. Phizackerley, S. M. Soltis, P. Kuhn, *J. Synchrotron Radiat.* 2002, **9**, 401-406.
3. N. P. Cowieson, D. Aragao, M. Clift, D. J. Ericsson, C. Gee, S. J. Harrop, N. Mudie, S. Panjikar, J. R. Price, A. Riboldi-Tunnicliffe, R. Williamson, T. Caradoc-Davies, *J. Synchrotron Radiat.* 2015, **22**, 187-190.
4. D. Aragao, J. Aishima, H. Cherukuvada, R. Clarken, M. Clift, N. P. Cowieson, D. J. Ericsson, C. L. Gee, S. Macedo, N. Mudie, S. Panjikar, J. R. Price, A. Riboldi-Tunnicliffe, R. Rostan, R. Williamson, T. T. Caradoc-Davies, *J. Synchrotron Rad.* 2018, **25**, 885-891.
5. G. Sheldrick, *Acta. Crystallogr. A* 2008, **64**, 112-122.
6. G. Sheldrick, *Acta. Crystallogr. A* 2015, **71**, 3-8.
7. G. M. Sheldrick, *Acta. Crystallogr. C* 2015, **71**, 3-8.
8. L. J. Barbour, *J. Supramol. Chem.* 2001, **1**, 189-191.
9. O. V. Dolomanov, L. J. Bourhis, R. J. Gildea, J. A. K. Howard, H. Puschmann, *J. Appl. Crystallogr.* 2009, **42**, 339-341.
10. A. L. Spek, *Acta. Crystallogr. C* 2015, **71**, 9-18.